Acoustical observation of bubble oscillations induced by bubble popping

Junqi Ding,[1,*] Felicia W. Tsaur,[1] Alex Lips,[1] and Adnan Akay[2]
[1]*Unilever Research & Development, 40 Merritt Boulevard, Trumbull, Connecticut 06611, USA*
[2]*Department of Mechanical Engineering, Carnegie Mellon University, Pittsburgh, Pennsylvania 15213-3890, USA*
(Received 17 May 2006; published 3 April 2007)

Acoustic measurements of aqueous foams show three distinct radiation mechanisms that contribute to the sound pressure field: oscillations of a bubble surface that precede popping due to the instability of thin liquid film, impulsive radiation due to bursts of bubbles, and oscillations from neighboring bubbles excited by a burst bubble. The movies captured by a fast camera confirm that the bubbles adjacent to a breaking bubble oscillate under the influence of the pressure generated by the burst bubble. The spectra of resulting transient sounds fall in the range of 2–8 kHz and those from bubble oscillations correlate well with the bubble size.

DOI: 10.1103/PhysRevE.75.041601 PACS number(s): 68.15.+e, 82.70.Rr, 83.80.Iz

INTRODUCTION

Aqueous foams play very important roles in both daily life and industrial processes [1,2]. Shampooing hair, washing dishes, taking a bath, pouring beer, and producing and transporting oil are a few examples. Personal wash products—for example, foam properties such as the ability to initiate its formation, bubble growth and foam coalescence, rheological behavior and bubble size distribution, stability and collapse—are all related to the consumers' "in-use" perceptions. The collapse or burst of bubbles is a particularly important subject that continues to attract scientific interest even after decades of studies, in part because of the noise produced by foams [2–4]. The characteristics of sound generated by bubbles can reveal important information about the collapse or burst mechanism and the properties of the fluid-gas mixture [5–11].

The life of a foam is determined by the thinning (drainage) [12] and breaking (coalescence or collapse) of the thin fluid walls. The deconstruction of thin fluid films is very important in many technological applications and in many physical and biological thin-film phenomena [13–22]. The spontaneous film rupturing due to film thinning caused by gravity in surfactant foams requires an activation energy of the order of σh^2, where σ is the interfacial tension and h the thickness of the film [13,14]. The film is not expected to burst until its thickness is, for a system with interfacial tension of about 20 mN/m, down to about 10 nm. However, because the critical thickness for spontaneously rupturing is usually larger than 10 nm, sustained surface fluctuations that amplify become necessary to overcome the energy barrier. Reiter *et al.* [18] applied a real-time optical microscope to study the destruction of polymeric films and found four distinct stages for film destruction, confirming the theoretical prediction for the surface fluctuations. These are amplification of surface fluctuations, breakup of the film and formation of holes, growth and coalescence of holes, and droplet formation and ripening. The instability of thin liquid films and the resulting amplification of surface fluctuations have been explained theoretically, but the experimental verification has been confined to polymeric films [18], in part because it is very difficult to visualize surfactant thin films with regular optical methods—for instance, with a microscope.

This communication reports on the measurement of sound radiation from bubbles in foams resulting from their oscillations and bursts, and relates these sounds to the destruction mechanism of the bubbles. By measuring and analyzing the acoustic emissions from foams generated with different bubble size distributions, three distinct sources are identified that contribute to the acoustic pressure: growing thin-film vibration amplitude preceding the burst of a bubble, the popping or the bursting of a bubble, and the oscillations from the neighboring bubbles excited by the transient pressure from a burst bubble. The growing thin-film vibrations preceding the burst of a bubble were also observed on top of a single bubble on a needle and are related to the surface fluctuations which lead to the breakup of the liquid film on the top of bubble as observed in polymeric films [18]. In addition, reflections from the foam surface or other surfaces also contribute to the sound measurements. For foams with a wider distribution of bubble radius (approximately 50–600 μm, with a mode radius around 600 μm), the sound pressure frequency distribution ranges between 2 and 8 kHz. For foam with smaller mode radius and narrower distribution, the spectrum bifurcates and a second peak develops in its envelope, while the first peak in the envelope of the spectrum between 2 and 8 kHz remains nearly intact. As the mode radius is further decreased, the second peak shifts to a higher-frequency range. The second peak correlates well with the predicted natural frequencies of bubble oscillations. The first peak in the frequency spectrum is associated with bubble burst and has similar wave forms to impulsively generated sounds, such as those by laser sparks. The movies captured by a fast camera confirm that the bubbles adjacent to a breaking bubble oscillate under the influence of the transient wave generated by the burst.

FOAM PREPARATION

Only a few studies are reported in the literature on foam generation techniques (shaking, air blowing, etc.) [1,23]. Recently Caps *et al.* [24] studied the foaming dynamics in

*Author to whom correspondence should be addressed. FAX: 203-381-5495. Electronic address: Junqi.Ding@unilever.com

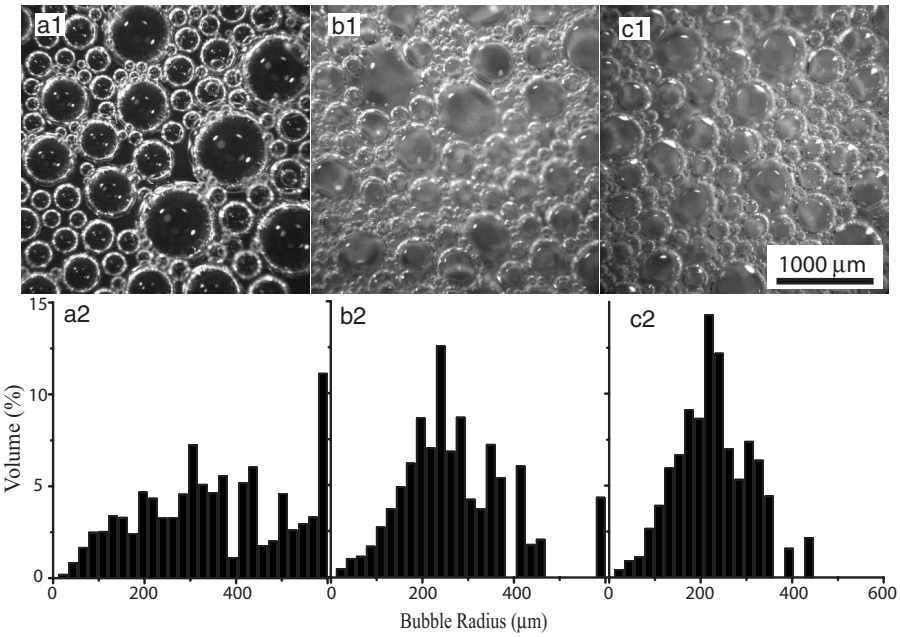

FIG. 1. Micrographs and size distributions of SDS foams prepared by different breakdown speeds [gas fraction=90%; breakdown speed: (a) 217 rpm, (b) 1400 rpm, and (c) 2300 rpm. For our discussion, we will use samples *A*, *B*, and *C* to label those three foam samples throughout this paper, respectively]. All micrographs were snapshots at 5 min after transferring foams into Petri dishes. The size distributions shown in (a2), (b2), and (c2) were obtained by counting at least five micrographs for each foam sample to minimize the error. By increasing the breakdown speed, a foam sample with smaller-size bubbles and narrower distributions can be produced.

Hele-Shaw cells and found that as a function of the number of the upside-down flips, an increasing number of bubbles composes the foam, until saturation is observed. In this study, we combined "shaking" and "shearing" methods to generate foams. Foams with different size distributions and mode radius were generated in two steps. First, the foam with large size bubbles was produced by shaking solutions of sodium dodecyl sulfate (SDS, ultrapure, ICN Biomedicals, Inc., Aurora, OH) at just above its critical micellar concentrations (CMCs) in a closed container with a fixed volume for 30 sec. In the second stage, the large-radius bubbles were broken down to smaller-size bubbles by applying a suitable stirring (or breaking-down) speed (Tekmar RW20DZM, Cincinnati, OH) for a prescribed time.

Foam samples with the desired size and gas fraction were produced by adjusting the stirring or breakdown speeds (between 217 rpm and 2500 rpm which are the low- and high-speed limits for the instrument) and the initial volume of solution. The foam was then immediately transferred into a Petri dish and imaged using an optical microscope (Leica Wild M420, Bannockbum, IL). For statistical purposes, multiple surface images of different locations were taken immediately after transferring the foam into the Petri dish and 5 min and 10 min afterwards, respectively. Figure 1 shows the micrographs of three typical foam samples with a fixed gas fraction of 90% at 5 min after transferring (in the rest of this paper, the three foam samples will be designated as *A*, *B*, and *C*). The breakdown speed of 217 rpm was used to generate foam sample *A*, while breakdown speeds of 1400 rpm and 2300 rpm were used for generating samples *B* and *C*, respectively. Multiple images were used to obtain the size distribution for each foam sample. Figure 1 also presents the size distributions for the foam samples *A* [Fig. 1(a2)], *B* [Fig. 1(b2)], and *C* [Fig. 1(c2)]. With this method, the foam samples with targeted size characteristics could be reliably reproduced. Increased breakdown speeds yielded foam samples with smaller-size bubbles and smaller standard deviation.

As pointed out by Caps *et al.* [24], foam generation is a complex process with very few descriptions reported in the literature. While a consumer can easily generate a "creamy" lather by applying "shear" when using personal wash products, it is very difficult to emulate the same process and, to our knowledge, no such apparatus exists that can simulate the human lathering process. Experiments point to the surfactant or surfactant mixture systems, the initial surfactant solution concentrations, the gas fraction, and the method used, all contributing to the foam generation and foam properties. For the SDS system with the concentration just above its CMC, without the shearing (breaking-down) step, the foam resulted from shaking drains pretty fast. With increasing shearing (breaking-down) rate, the foam viscosity increases (data not shown) and the drainage rate decreases drastically. By increasing the shearing rates, in addition to generating more stable foam systems, the percentage of large bubbles decreases, which indicates that the shearing process breaks down the larger bubbles. However, the percentage of small bubbles does not increase significantly, which indicates that coarsening must not be ignored during the foam generation. We also applied the same method to other surfactant systems and surfactant mixture systems, and found that the size and distribution of bubbles depend not only on the shearing speed but also on the surfactant systems. For a particular surfactant system, there must be a limit for the bubble size as in the SDS system, the mode radii of samples *B* and *C* are very close even with the shearing speed increased from 1400 rpm to 2300 rpm. This is consistent with the saturation effect of the number of bubbles with increasing upside-down flips observed by Caps *et al.* [24]. The two-step method is not an ideal method to make a monodisperse foam system, but it generates foams that closely resemble the lather generated by the consumers.

SOUND MEASUREMENTS

Two types of acoustic measurements were conducted: one to investigate the sound field of a foam and the other to

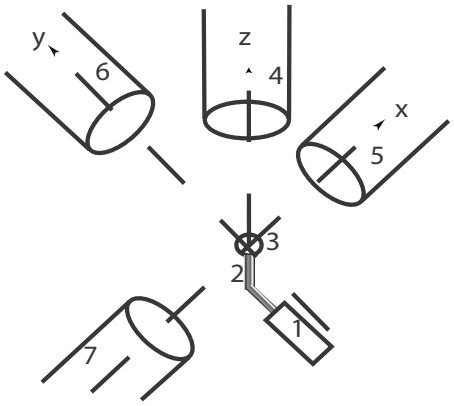

FIG. 2. Schematic diagram for the setup of measuring single bubble burst. 1: Syringe with SDS solution. 2: Stainless steel needle (flat tip). 3: single bubble. 4–7: microphones at different angles. Considering the bubble located at the origin of a Cartesian coordinator system, the *xy* plane is the horizontal plane; microphones 5 and 7 are on the *x* axis, microphone 4 is on the *z* axis, and another side microphone 6 is on the *y* axis.

examine the radiation from a single isolated bubble. In the first set, the foam samples with desired size characteristics were placed in a Petri dish and the emitted sounds were measured for at least 10 min with two microphones located above the foam samples. In the second set, as shown in Fig 2, a single bubble was generated by pumping a surfactant solution inside a syringe to simultaneously measure the acoustic pressure of the single bubble burst from different angles. Four microphones were positioned above and at the sides of the breaking bubble to examine the directional characteristics of the emitted sound. The sound pressure signals were recorded using a data acquisition system (pulse system with modules type 3032A and type 7533, Brüel & Kjaer, Norcross, GA) at an acquisition rate of 65 536 Hz. To minimize the effects of ambient noise, measurements were carried out in a sound isolation enclosure (SE2000 series, Whisper Room Inc., Morristown, TN) that effectively insulates most of the higher-frequency components (above 1000 Hz).

FREQUENCY ANALYSIS

A proprietary software package written with Microsoft Visual C++, which calls the signal processing functions from MATLAB (Mathworks, Natick, MA), was used to analyze the acoustic signal. Since a 10-min-long unprocessed sound pressure datum contains nearly 40×10^6 data points, it is impractical to perform a fast Fourier transfer (FFT) of the entire signal at one time. Because of this concern, the 10-min-long acoustic signal was reduced into smaller samples, with each sample containing 10-sec signal and 655 K data points. To include a larger amount of bubbles, we averaged every 10 consecutive FFT results to represent the frequency behavior of acoustic emission in the 100-sec period—e.g., FFT results for signal from 0 to 100 sec, from 100 to 200 sec, and so on. Although the FFT results showed slight changes from period to period, the general characteristics of the spectra remained the same.

OBSERVATIONS: SOUND MEASUREMENT RESULTS

Typical acoustic emission after filtering with a fourth-order Butterworth high-pass filter (cut off frequency 500 Hz) has high-amplitude, short-duration pulses in the sound pressure signal which are related to the bubble burst events (data not shown). This is very similar to the acoustic profiles reported in the literature [8], but with fewer bubble popping events. With an increase in the breakdown speeds, the bubble popping events reduce. For sample *A*, it only took around 15 min for all bubbles in a Petri dish to disappear while it took around 50 min for all bubbles in sample *C* to disappear. In a given sample, the frequency of bubble popping events following the formation of a foam is not uniform due to the avalanches of popping bubbles [8,25]. Bubbles burst at a very fast rate in the first 50 sec and then slow down. The potential influence of such transient effects on acoustic measurements is reduced by taking measurements between 100 and 600 sec following the foam sample generation, with particular focus on the time period between 300 and 400 sec during which foam sample reaches a quasistable state. To better examine the nature of bubble burst events, the sound pressure from single bursts was plotted with an expanded time scale for each of the three samples generated. Figures 3(a)–3(c) show typical acoustic profiles for samples *A*, *B*, and *C*, respectively. In these figures, for easier comparison, the time axis was shifted to begin at 0 msec for each signal. Similar to those reported in the literature [8], single-burst events dominate the pressure field from a foam (more than 95% of the total burst events) although double bursts and multiple bursts can be occasionally observed. The typical duration of each individual bursts lasts about 1–2 msec.

The spectrum of sound emission from a foam strongly depends on the size distribution and mode radius of bubbles. The left column in Fig. 4 shows the power spectral density for foam samples *A*, *B*, and *C* each for the periods from 300 to 400 sec following sample generation. For foam sample *A*, which has a broader bubble size distribution and with larger bubble mode radius, the sound pressure frequencies fall between 2 and 8 kHz. The power spectrum density exhibits a corresponding broad distribution within this range. As the mode radius of foam becomes smaller (samples *B* and *C*), the spectrum bifurcates and two major peaks develop in the power spectral density. The peak between 2 and 8 kHz remains similar in distribution with slight shifts while the second peak shifts to a higher-frequency range as the mode radius decreases (sample *C*).

The bubble burst events and the following behaviors of the sample were visualized using a fast camera (Redlake MotionXtra HG-100K, San Diego, CA) at an acquisition rate of 10 000 frames per second (fps). At this resolution, the bubble popping and the ensuing shock wave that deforms the bubbles next to the popped bubble were clearly visible. Figure 5 shows two micrograph sequences of bubble popping and the response of the nearby bubbles in two foam samples. The movies with different playback speeds are also provided [26]. As observed in Fig. 5 and the movies, the different foam samples showed similar bubble bursts, but different behaviors following the bursts. For sample *A*, the popping bubble causes the bubbles nearby to be dislocated and de-

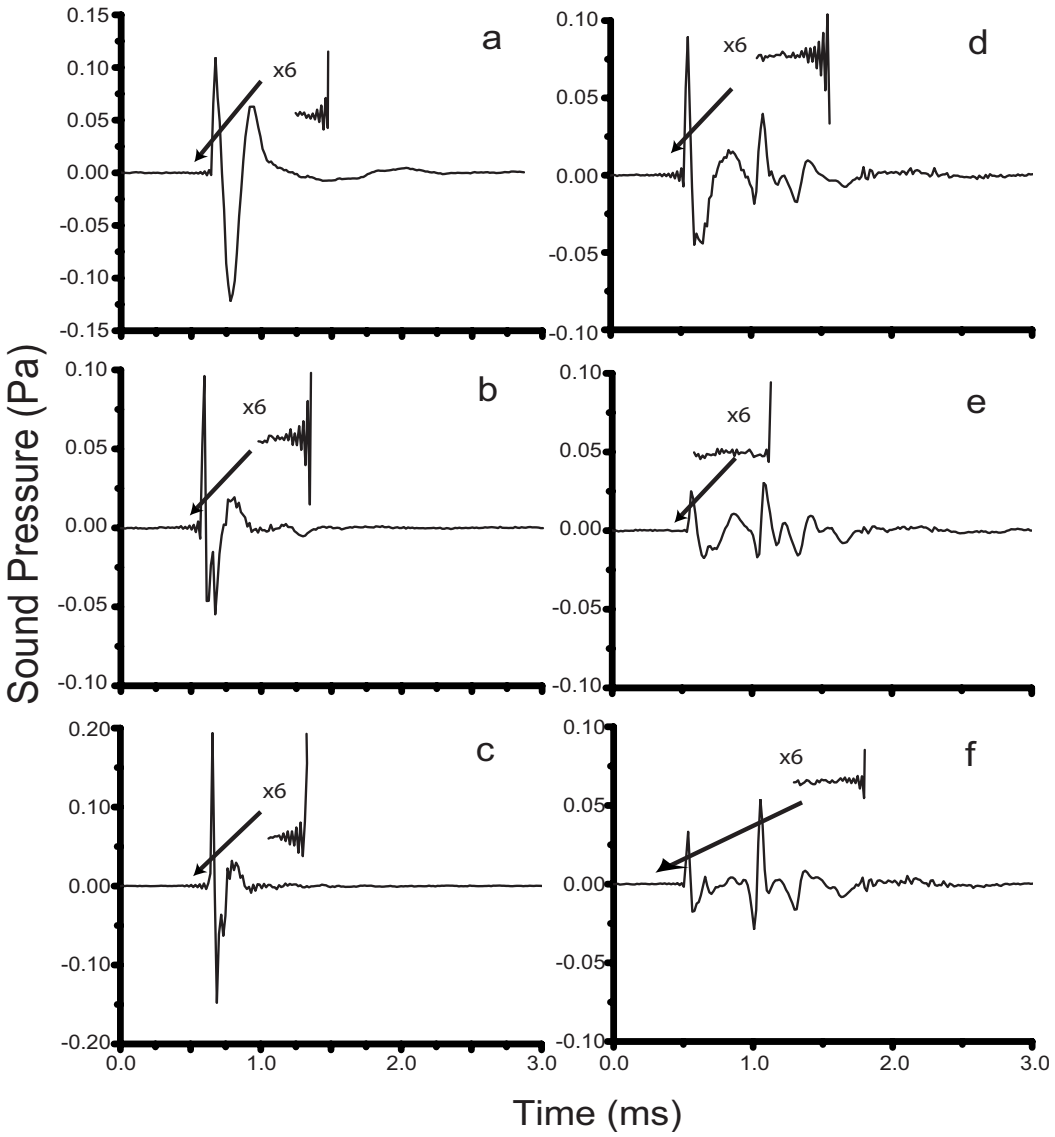

FIG. 3. Typical acoustic signals of a single-bubble burst for SDS foam samples [(a) sample *A*, (b) sample *B*, and (c) sample *C*] and for a single bubble from different angles [(d) +*z*, (e) +*x*, and (f) +*y*. Refer to Fig. 2 for the *xyz* position]. For easy comparison, each signal was shifted to the beginning of 0 msec.

formed, while in sample *C*, since the rigid network formed by the nearby bubbles constrains the movement of the bubbles, the burst bubble causes the bubbles nearby to deform with very limited dislocation, which forces the bubbles to oscillate. The deformed bubbles oscillate as they migrate into the empty space created by the popped bubbles but at a slower speed. However, the fast camera did not capture the interference rings that move around rapidly on top of the bubbles immediately prior to their burst as discussed below.

The first peak in the power spectral density plots which weakly depends on the bubble size is apparently related to the bubble bursts. The authors suggest that the second peak in the plots which is strongly related to the bubble size can be explained by the oscillations from the bubbles next to the popping bubbles. Predictive models for bubble freely oscillating in a liquid have been discussed extensively in literature [2,4–6,27]. For small-amplitude oscillations of a permanent gas (noncondensable) bubble in a liquid for which vapor effects can be neglected, the natural frequency f_0 is given by

$$f_0 = \frac{1}{2\pi}\sqrt{\frac{3\kappa P_0}{\rho R_0^2} - \frac{2\sigma}{\rho R_0^3}}, \tag{1}$$

where κ is the gas polytropic component which equals γ, the ratio of specific heats of the gas if the pressure-volume relationship of the gas is taken to be adiabatic; P_0 is the ambient pressure, R_0 is the nominal radius, σ is the surface tension, and ρ is the liquid density. If the surface-tension effects are neglected, for air bubbles (for which γ=1.4) in water under standard conditions, the natural frequency of a bubble with a nominal radius R_0 in meters can be estimated by a simpler equation

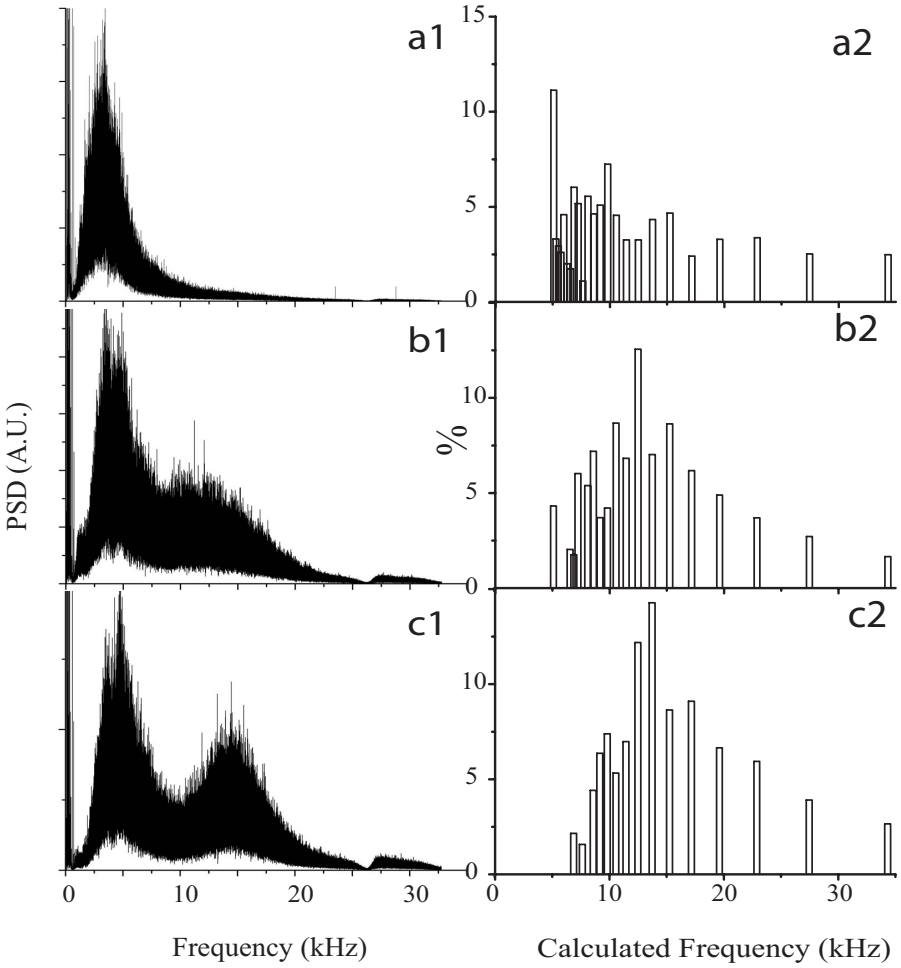

FIG. 4. FFT spectra of the acoustic emissions from SDS foam samples [(a1) sample *A*, (b1) sample *B*, and (c1) sample *C*] and calculated frequency spectra by assuming the bubble oscillation based on the size distributions from Fig. 1 [(a2) sample *A*, (b2) sample *B*, and (c2) sample *C*].

$$f_0 \approx \frac{3}{R_0}(Hz). \tag{2}$$

The second column in Fig. 4 presents the predicted frequencies of pressure radiated from oscillations of bubbles obtained by applying Eq. (2) to the size distribution data shown in Fig. 1 for different samples.

Comparison of the calculated frequency spectra with the experimental frequency spectra (the second column and the first column, respectively, in Fig. 4) shows a strong correlation between the second distribution peak in the measured frequency spectra and the calculated frequency spectra based on the bubble oscillation model.

Equations (1) and (2) do not adequately describe the foam samples described above since they do not take into account the following conditions: the bubbles are not freely oscillating and the surrounding medium is not a pure liquid that has the density of water. The effective density of the surrounding medium in the present case is much smaller than the density of water but larger than the liquid fraction of the foam. As a result, Eq. (2) underestimates the oscillation frequency. On the other hand, the surrounding medium, as observed by the fast camera, slows down the dislocation of the nearby bubbles in the samples at higher breaking-down speeds, constraining the freely oscillating bubbles, thus effectively damping their oscillation frequency [4]. In this case, Eq. (2) overestimates the oscillation frequency. In addition, considering all possible sources of acoustic emissions from the foam systems used, we cannot find other causes except the oscillations which relate to bubble sizes and the shifted second frequency peak in the power spectral density plots. Therefore, it is reasonable to assume that the natural frequency of the oscillating bubbles in foam samples is not far from the estimated frequency based on Eq. (2). An in-depth understanding of these two effects needs further work.

The part of the sound spectra of the foam samples [(a1), (b1), and (c1) in Fig. 4] from the foams that fall above 25 kHz with small amplitudes is independent of the size distribution characteristics of the foam samples. The frequency is surprisingly high since most popping bubbles have larger radii and the natural frequency for those larger bubbles is much smaller ($<$25 kHz) than the observed frequency range ($>$25 kHz), suggesting a different mechanism as the cause. Our observations suggest that these high-frequency components are related to the higher-frequency oscillations that precede each bubble burst. As shown in the enlarged figures in Figs. 3(a)–3(c), the oscillations that precede each bubble burst have amplitudes that increase exponentially as they reach the burst event and period that corresponds to around 30 kHz.

To identify the source of this acoustic emission, we designed an experiment, as shown in Fig. 2, to record the acoustic responses of a single-bubble burst at the tip of a

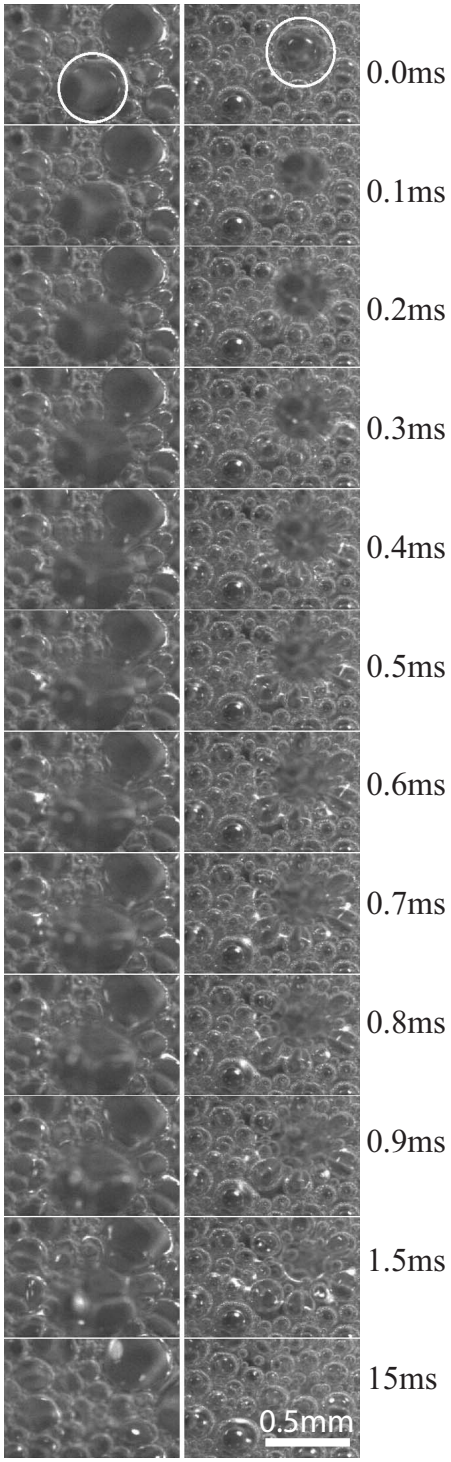

FIG. 5. Micrographs show a time sequence of popping bubbles and their neighbors in two foam samples (left column, sample *A*; middle column, sample *C*) captured by a fast camera at different moments. The popping bubble in each sequence is marked with a circle in the first frames. As a consequence of the bubble bursts, the bubbles near the popping bubble are deformed and oscillated in sample *C*, while the nearby bubbles are dislocated under the shock of bubble popping in sample *A*.

needle at different directions simultaneously. A single-bubble system prevents contributions from multiple-bubble sources such as bubble oscillations induced by popping bubble and coalescence. A set of measurements recorded sound pressure from a single bubble [Figs. 3(d)–3(f)], isolating the impulsive nature of the sound radiated, including acoustic emissions that develop prior to the burst. As in the cases of three foam samples, the isolated single bubbles also show a very similar acoustic pattern. The burst generates a compressive pressure pulse followed by a rarefaction, which can have a longer period and lower amplitude than the compressive peak depending on the size of the bubble. The acoustic profile from the microphone above the bubble is different from the acoustic pressure histories from the other microphones located in the same horizontal plane as the bubble. The preceding acoustic emission appears directly above the burst bubble, but difficult to observe in other directions. This suggests a pistonlike radiation from a small part of the top surface of the bubble, followed by the compressive sound pressure observed in all bursts.

The reason for the burst to develop at the top of the bubble, and to act as a pistonlike radiator, rests with the drainage mechanism. The drainage of liquid on a bubble creates a thinner top part, and this leads to the spontaneous breakup of the bubble as the thickness of the top reduces to a critical thickness [18,21,22]. The spontaneous film rupturing requires a high activation energy if the film thickness is larger than 10 nm [13,14]. It has been predicted theoretically [13–16,19,28] that the small surface fluctuations can be amplified to overcome the energy barrier, as was confirmed for polymeric films [17,18,29,30]. The hole formed at the top of the bubble and then rapidly expanded. The rates at which the hole expands are dependent on the film systems [21,22,31]. The higher pressure inside the bubble is released from the hole while the hole forms and expands. It is not surprising to observe pistonlike radiation from the top of the breaking bubble while the amplitudes of the acoustic emissions from horizontal microphones are much less. The initial sound pressures detected from all directions are positive, which indicates that the bubble film expands to all directions during the bubble collapse.

An important remaining question relates to the behavior of the bubble before it bursts and generates high-frequency acoustic emissions, particularly at its top. One important feature of the observed processes was the formation of interference patterns just before the bubble burst, indicating that the bubble film breaks at the thickness of the range of light wavelength, which is much thicker than 10 nm. As predicted by theory, there is a large energy barrier to overcome if the film ruptures at a film thickness more than 10 nm. In addition, unlike the system reported in the literature [22], the interference patterns that appeared in our systems were moving around on the top of bubble very rapidly. This observation suggests the possible mechanism of surface oscillations that precede a bubble burst to be an instability. Whether the initial surface oscillations result from thermal fluctuations or long-range interactions is not clear, but the observations show clearly that the sound pressure amplitude from these oscillations increases exponentially, resulting in the burst of the bubble. Considering that the thermal energy can only overcome the activation energy of hole formation for a very thin film [13,32], the exponential oscillations which lead to the bubble burst must come from the van der Waals interac-

tions predicted by theory [14]. This behavior is similar to that observed in polymeric films observed by Reiter *et al.* [18]. The confirmation of the contribution from the long-range interactions needs further research. In aqueous foams, as a result of drainage, the top surface of the foam becomes dry and the bottom becomes wet, resulting in a thinning of the top part of a bubble. As the film becomes thinner, it oscillates with exponentially increasing amplitude, which can further contribute to the drainage process, thus making it even thinner, prior to its burst, setting up an instability mechanism. The amplification of the surface oscillations (or surface fluctuations, or both) eventually leads to the breakup and subsequent bubble burst.

The sound generation mechanisms from a foam sample can be summarized as follows. An individual bubble in a foam sample drains, and as its top wall becomes thinner, the top film starts to oscillate under the influence of thermal fluctuations or long-range interactions. Oscillations lead to further drainage, setting up an instability that further increases the oscillation amplitude at the top of the bubble until a hole is generated and the bubble bursts. The burst generates the impulsive wave, which also excites other bubbles adjacent to the breaking bubble.

Thus, in addition to the reflections from the foam surface, three distinct sources contribute to the direct field of the measured acoustic pressure: thin-film oscillation which precedes the bubble burst, the bubble burst, and oscillations from the nearby bubbles excited by the burst bubble. The movies captured by a fast camera confirm that the bubbles adjacent to the breaking bubble oscillate under the influence of the wave generated by the burst bubble.

ACKNOWLEDGMENTS

Technical support from Liang Tsaur, P.J. Singh, and Junqing Chen is highly appreciated. We thank Howard Stone for helpful discussions and suggestions and N. Vandewalle for providing us with reprints.

[1] D. Weaire and S. Hutzler, *The Physics of Foams* (Oxford University Press, New York, 1999).
[2] D. Lohse, Phys. Today **56**(2), 36 (2003).
[3] Lord Rayleigh, Philos. Mag. **34**, 94 (1917).
[4] C. E. Brennen, *Cavitation and Bubble Dynamics* (Oxford University Press, New York, 1995).
[5] T. G. Leighton, *The Acoustic Bubble* (Academic Press, San Diego, 1994).
[6] A. Prosperetti and H. N. Oguz, Annu. Rev. Fluid Mech. **25**, 577 (1993).
[7] D. E. Spiel, J. Geophys. Res., [Oceans] **97**, 11443 (1992).
[8] N. Vandewalle, J. F. Lentz, S. Dorbolo, and F. Brisbois, Phys. Rev. Lett. **86**, 179 (2001).
[9] N. Vandewalle, H. Caps, and S. Dorbolo, Physica A **314**, 320 (2002).
[10] N. Vandewalle and J. F. Lentz, Phys. Rev. E **64**, 021507 (2001).
[11] R. Manasseh, A. Nikolovska, A. Ooi *et al.*, J. Sound Vib. **278**, 807 (2004).
[12] S. A. Koehler, H. A. Stone, M. P. Brenner, and J. Eggers, Phys. Rev. E **58**, 2097 (1998).
[13] A. J. de Vries, Recl. Trav. Chim. Pays-Bas **77**, 383 (1958).
[14] A Vrij, Discuss. Faraday Soc. **42**, 23 (1966).
[15] A. Sheludko, Adv. Colloid Interface Sci. **1**, 391 (1967).
[16] M. B. Williams and S. H. Davis, J. Colloid Interface Sci. **90**, 220 (1982).
[17] G. Reiter, Science **282**(5390), 888 (1998).
[18] G. Reiter, R. Khanna, and A. Sharma, J. Phys.: Condens. Matter **15**, S331 (2003).
[19] A. Sharma and R. Khanna, Phys. Rev. Lett. **81**, 3463 (1998).
[20] S. Herminghaus, K. Jacobs, K. Mecke *et al.*, Science **282**, 916 (1998).
[21] N. D. Denkov, P. Cooper, and J. Y. Martin, Langmuir **15**, 8514 (1999).
[22] G. Debregeas, P. G. de Gennes, and F. Brochard-Wyart, Science **279**, 1704 (1998).
[23] R. J. Pugh, Adv. Colloid Interface Sci. **64**, 67 (1996).
[24] H. Caps, N. Vandewalle, and G. Broze, Phys. Rev. E **73**, 065301 (2006).
[25] W. Muller and J. M. di Meglio, J. Phys.: Condens. Matter **11**, L209 (1999).
[26] See EPAPS Documents No. E-PLEEE8-75-068704 for four movies from fast camera images. For more information on EPAPS, see http://www.aip.org/pubservs/epaps.html
[27] M. S. Plesset and A. Prosperetti, Annu. Rev. Fluid Mech. **9**, 145 (1977).
[28] A. Sharma, Langmuir **9**, 3580 (1993).
[29] G. Reiter and R. Khanna, Phys. Rev. Lett. **85**, 2753 (2000).
[30] G. Reiter and R. Khanna, Langmuir **16**, 6351 (2000).
[31] R. da Silveira, S. Chaieb, and L. Mahadevan, Science **287**, 1468 (2000).
[32] A Vrij and J. Th. G. Overbeek, J. Am. Chem. Soc. **90**, 3074 (1968).